Article

Investigation of Drug-Induced Hepatotoxicity and Its Remediation Pathway with Reaction Based Fluorescent Probes

Dan Cheng, Wang Xu, Lin Yuan, and Xiao-Bing Zhang

Anal. Chem., **Just Accepted Manuscript** • Publication Date (Web): 19 Jun 2017

Investigation of Drug-Induced Hepatotoxicity and Its Remediation Pathway with Reaction Based Fluorescent Probes

Dan Cheng[†], *Wang Xu*[†,//], *Lin Yuan**[†], *Xiaobing Zhang*[†]

[†]State Key Laboratory of Chemo/Biosensing and Chemometrics, College of Chemistry and Chemical Engineering, Hunan University, Changsha 410082 (PR China)

[//]*Current address: Department of Chemistry, Stanford University*

[*]Email: lyuan@hnu.edu.cn. Fax: +86-731-88821894

Abstract: Drug-induced liver injury (DILI) is considered a serious problem related to public health, due to its unpredictability and acute response. The level of peroxynitrite ($ONOO^-$) generated in liver has long been regarded as a biomarker for the prediction and measurement of DILI. Herein we present two reaction based fluorescent probes (**Naph-ONOO$^-$** and **Rhod-ONOO$^-$**) for $ONOO^-$ through a novel and universally applicable mechanism: $ONOO^-$ mediated deprotection of α-keto caged fluorophores. Among them, **Rhod-ONOO$^-$** can selectively accumulate and react in mitochondria, one of the main sources of $ONOO^-$, with a substantial lower nano-molar sensitivity of 43 nM. The superior selectivity and sensitivity of two probes enable real-time imaging of peroxynitrite generation in LPS-stimulated live cells, with a remarkable difference from cells doped with other interfering ROS, in either one-photon or two-photon imaging mode. More importantly, we elucidated the drug-induced hepatotoxicity pathway with **Rhod-ONOO$^-$**, and revealed that CYP450/CYP2E1-mediated enzymatic metabolism of acetaminophen leads to $ONOO^-$ generation in liver cells. This is the first time to showcase the drug induced hepatotoxicity pathways using a small molecule fluorescent probe. We hence conclude that fluorescent probes can engender a deeper understanding of reactive species and their pathological revelations. The reaction based fluorescent probes will be a potentially useful chemical tool to assay drug induced hepatotoxicity.

Introduction

Drug-induced liver injury (DILI) is the most common concern of acute liver failure, accounting for a substantial portion of acute hepatitis.[1,2] The emergence of DILI is complicated and its evaluation is difficult, as its clinical manifestation includes all pathological symptoms related to liver.[3] The estimated annual incidence of DILI is between 10 and 15 per 10,000 to 100,000 persons, a sample size too large to cover during clinical trials.[4] Hence this phenomenon also widely affects the pharmaceutical industry, leading to drug withdrawal even after released into the market.[5] Innovative preclinical hepatotoxicity screening methods could help examine hepatotoxicity during drug development; however, the development is proved to be complicated because many biomarkers exist during DILI process.[6-8] The lack of a straightforward, preclinical screening assay is also an issue.

Epidemiological studies reveal that reactive radicals are the main side-products of drug metabolism in liver and led to a range of cell apoptosis and other acute liver damages.[2] For example, acetaminophen (APAP), a pain killer and fever reducer common found on the market, is well-known to cause serious hepatotoxicity among certain population.[9] In the liver, APAP undergoes enzymatic biotransformation and generates reactive radicals, such as peroxynitrite ($ONOO^-$), through either one- or two-electron oxidation processes.[10,11] Since such enzymatic biotransformation universally exists among a wide range of drugs, $ONOO^-$ can therefore serve as a useful biomarker for detecting and studying drug-induced hepatotoxicity.[12] As the adduct of nitric oxide (NO) and superoxide radical ($O_2^{\bullet-}$), $ONOO^-$ is known to react with a wide array of biomolecules, such as proteins, lipids, and nucleic acids, causing disruption of cellular structure and functions and finally leading to cell death.[13,14] While generated in liver, elevated levels of

endogenous $ONOO^-$ often indicate acute hepatocellular damage.[15] Despite the fact that $ONOO^-$ tracing is crucial for both pathological and clinical studies, it has proved to be a tough target to monitor. The extremely short half-lives of $ONOO^-$ (less than a second, ~10 ms) almost precludes its detection after extraction, necessitating *in situ* monitoring upon formation.[16,17] Thus, it is a grand and urgent challenge in modern pharmaceutical industry to monitor $ONOO^-$ in real time.

In this work, we investigated the production and remediation pathways of drug induced hepatotoxicity in live cells using a newly designed, reaction based fluorescent probe. Since the emergence of fluorescence imaging technique, it has not only greatly enhanced the efficiency of preclinical studies, but also enabled a non-invasive, powerful and clinically translatable way for tracing the progression of drugs' action and evaluating the extent of damages in real-time.[18-26] So far, there are a number of fluorescent probes for $ONOO^-$,[27-38] most of which rely on $ONOO^-$ mediated oxidation that releases ketone end groups. Although some of these probes have been used for biomedical studies,[39-41] there are very limited examples targeting drug-induced hepatotoxicity.[42,43] Our probe exploits an brand new reaction: $ONOO^-$ mediated deprotection of α-ketoamide, in which an $ONOO^-$-triggered nucleophilic attack at the α-carbonyl group leads to the dissociation of di-keto group. Hence by linking a fluorophore and a quencher with the α-ketoamide group, we formulate a selective and sensitive fluorescent turn-on probe for $ONOO^-$. As far as we know, this is not only a demonstration of new reaction based $ONOO^-$ fluorescent probe, but also a novel study of drug induced hepatotoxicity pathways using small molecule fluorescent probes.

Experimental Section

Materials and General Experimental Methods. For details, see the Supporting Information**.**

Synthesis of Naph-ONOO$^-$/Rhod-ONOO$^-$. Compounds **Naph-NH$_2$/Rhod-NH$_2$** was prepared by reported method.[44,45] A mixture of compound 4-nitrophenylglyoxylic acid (19.5 mg, 0.1 mmol), HATU (38.0 mg, 0.1 mmol) and triethylamine (2 μL) in 1.5 mL anhydrous dichloromethane was stirred for 20 min, then compound **Naph-NH$_2$** (27.0 mg, 0.1 mmol) or **Rhod-NH$_2$** (48.6 mg, 0.1 mmol) was added under argon atmosphere. The mixture was stirred at room temperature for 2 hours. Then the solvent was removed under vacuum condition, and the mixture was purified by column chromatography on silica gel with (CH_2Cl_2/EtOH=60:1) to offer **Naph-ONOO$^-$** as a yellow solid (14.5 mg, 32.5%) or **Rhod-ONOO$^-$** as a red solid (8.4 mg, 12.7%). For **Naph-ONOO$^-$**: ^{1}H NMR (400 MHz, $CDCl_3$) δ 9.91 (s, 1H), 8.71-8.69 (5H), 8.40 (d, J = 7.9 Hz, 2H), 8.32 (d, J = 8.3 Hz, 1H), 7.88 (t, J = 7.5 Hz, 1H), 4.45 (t, J = 5.1 Hz, 2H), 3.75 (t, J = 5.1 Hz, 2H), 3.39 (s, 3H). ^{13}C NMR (100 MHz, $CDCl_3$) δ 184.3, 162.9, 156.9, 136.1, 135.6, 131.8, 131.2, 130.7, 126.4, 124.7, 122.7, 122.6, 118.6, 117.6, 68.6, 57.8, 38.4. HRMS (EI) $C_{23}H_{17}N_3O_7$ (M), calculated for 447.1057, found 447.1066. For **Rhod-ONOO$^-$**: ^{1}H NMR (400 MHz, MeOD + $CDCl_3$) δ 8.26 (d, J = 8.8 Hz, 2H), 8.02 (d, J = 7.8 Hz, 1H), 7.98 (d, J = 8.8 Hz, 2H), 7.82 (t, J = 2.1 Hz, 1H), 7.76 (dd, J = 8.0, 4.9 Hz, 1H), 7.70 (t, J = 7.4 Hz, 1H), 7.27 (d, J = 8.7 Hz, 1H), 7.20 (d, J = 7.5 Hz, 1H), 6.71 (d, J = 8.7 Hz, 1H), 6.57 (d, J = 8.8 Hz, 1H), 6.53 – 6.46 (2H), 3.42 (t, J = 7.0 Hz, 4H), 1.19 (t, J = 6.8 Hz, 6H). ^{13}C NMR (100 MHz, MeOD+$CDCl_3$) δ 170.4, 169.4, 153.1, 152.1, 150.1, 148.2, 147.1, 139.7, 134.9, 131.6, 129.7, 128.9, 128.7, 128.3, 127.6, 124.6, 124.1, 122.9, 115.6, 115.4, 115.4, 108.8, 108.0, 97.2, 78.2, 77.9, 77.5, 44.1, 11.2. HRMS (ESI) $C_{32}H_{26}N_3O_7^+$ (M^+), calculated for 564.1779, found 564.1776.

Fluorescence microscopic imaging of APAP-induced cell damage experiments. HepG2 cells were pretreated with APAP (0 - 500 μM, respectively) for 12 hours, and then incubated with 5.0

μM **Naph-ONOO$^-$** or **Rhod-ONOO$^-$** for 40 min. Cell imaging was carried out after washing the cells with PBS for three times.

The remediation of hepatoxicity in living cells. HepG2 cells were treated with 200 μM GSH for 1 hour, or 20 μM trans-1,2-dichloroethylene (*t*-1,2-DCE) for 2 hours or 160 μM 1-aminobenzotriazole (1-ABT) for 12 hours before drug treatment, respectively. Then the cells were treated with APAP (250 μM) for 12 hours, and then incubated with 5.0 μM **Rhod-ONOO$^-$** for 40 min before imaging.

Results and Discussion

Design and synthesis of fluorescent probes for ONOO$^-$. It is possible to design reaction based fluorescent probes for ONOO$^-$ owing to its strong nucleophilicity and oxidation capacity. Previous literature has reported that α-keto esters can react with ONOO$^-$ smoothly under physiological conditions (Scheme 1A).[27] Thus, we propose that deprotecting the α-keto caged fluorophore may generate a specific turn-on probe for ONOO$^-$. In fact, the protection/deprotection approach represents a new research focus for developing selective probes in biological systems.[46-51] The protection groups could play a crucial role in modulating fluorescence "off-on" status. Accordingly, we employed phenylglyoxylic acid to protect the amine group in the α-keto caged fluorophore. The α-ketoaminde protection of the amino group on the fluorophores weakens their π-conjugation via combined effects of internal charge transfer and photo-induced electron transfer. The result is the low fluorescence emission of the fluorophore scaffolds. Upon reaction with ONOO$^-$, the probe 1) undergoes a nucleophilic attack at a-keto position, forming an intermediate; 2) releases NO_2 species by intramolecular cyclization and generates highly reactive epoxide; 3) proceeds to intramolecular rearrangement to yield an anhydride, which hydrolyzes to dissociate

into a carboxylic acid and amino group (Scheme 1B).

Based on the known mechanism, we incorporated the a-ketoaminde group into two prominent chromophores, rhodamine and amino naphthalimide. They are linked with phenylglyoxylic units bearing simple electron-donating or withdrawing substituents, such as hydrogen, methoxy group, and nitro group at the *para*-position of the phenyl ring of phenylglyoxylic acid (Scheme 1C). These fluorescent probes were prepared through simple one-step reactions (for synthetic and characterization details, see the Supporting Information).

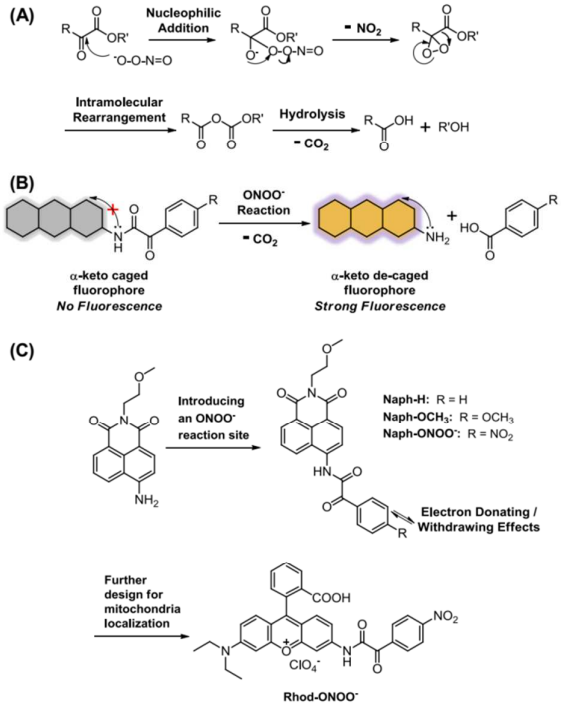

Scheme 1. (A) The proposed reaction mechanism of α-keto esters with $ONOO^-$. (B) The proposed reaction mechanism of α-keto caged fluorophore with $ONOO^-$. (C) Design of new fluorescent probes for $ONOO^-$.

To verify our proposed mechanism, we chose **Naph-ONOO$^-$** as the pilot compound and analyzed the reaction mixture of **Naph-ONOO$^-$** and peroxynitrite. Apart from the final major product **Naph-NH$_2$** with a mass of 269.2, we surprisingly found another peak at m/z = 418.2 (Figure S1). We propose that another intramolecular rearrangement may exist in the reaction process. $ONOO^-$ engages in a nucleophilic addition at α-keto and forms a dioxirane, which quickly

undergoes rearrangement to result in a reactive anhydride species. After anhydride forms, it is prone to release carbon dioxide and render a reaction intermediates that is stable enough to be captured by mass spectrometry: the amide product **Naph-1**. Then under aqueous condition the amide hydrolyzes to produce the final product, **Naph-NH_2** (Scheme S2). The capture of the intermediate can partially attribute to the slow kinetics of amide hydrolysis through reactions with external water molecules.

Spectral response of the probes to $ONOO^-$. We first examined their reactivity with $ONOO^-$ at physiological buffer conditions (PBS buffer solution, 25 mM, 1% DMF, pH 7.4). As shown in Figure S2, **Naph-H** and **Naph-OCH_3** displayed minor fluorescence enhancement after reaction with $ONOO^-$ while **Naph-$ONOO^-$** exhibited a more substantial fluorescence change within 0.5 hour, which indicates **Naph-$ONOO^-$** reacted faster with $ONOO^-$ than **Naph-H** and **Naph-OCH_3**, showing a kinectic advantage. We propose that the nitro group of **Naph-$ONOO^-$** can serve as a strong electron-withdrawing substituent, which enhances the electrophilicity of the *para* carbonyl group, as compared to the hydrogen atom of **Naph-H** and the methoxy group of **Naph-OCH_3**, respectively. Accordingly, we have also developed another $ONOO^-$ probe with potential mitochondria-targetable capacity based on rhodamine fluorophore, **Rhod-$ONOO^-$**, which has the same reaction site as **Naph-$ONOO^-$** (Scheme 1C).

In addition, after reaction with $ONOO^-$, the absorption maxima of **Naph-$ONOO^-$** shifts from 350 nm to 382 nm, whereas a green emission band at 546 nm appears concomitantly (Figure S3 and 1A). Linearity is observed between fluorescence intensity and $ONOO^-$ concentration (Figure S4). The fluorescence and absorbance spectra of **Rhod-$ONOO^-$** at a range of $ONOO^-$ concentrations were also recorded, shown in Figure 1C and S5. With an increasing $ONOO^-$

concentration (0-16 μM), the fluorescence intensity of **Rhod-ONOO$^-$** at 558 nm also increases to more than 14-fold. The fluorescent color also gradually changes from colorless to orange emission (Figure 1C, inset), a consequence of rhodamine recovery. The detection limits of both probes are in the lower-nanomolar range, with **Naph-ONOO$^-$** estimated to be 79 nM while **Rhod-ONOO$^-$** reaching 43 nM (Figure S4 and S6). The superior sensitivity of both probes ensures their usage in monitoring trace amounts of intracellular $ONOO^-$. Additionally, **Naph-ONOO$^-$** and **Rhod-ONOO$^-$** display weak fluorescence emission at pH 4.1–9.1, and exhibit dramatic fluorescence enhancement to $ONOO^-$ in pH 7.0–9.0, which are well consistent with the physiological pH range (Figures S7 and S8).

To measure the selectivity of **Naph-ONOO$^-$** and **Rhod-ONOO$^-$**, we examined both probes with a range of biologically relevant metabolites, including reactive oxygen species (ROS) (H_2O_2, HOCl, $O_2^{\bullet-}$, •OH, BuOO•), reactive sulphur species (RSS) (H_2S, H_2S_2, HSO_3^-, Cys, GSH), reactive nitrogen species (RNS) (HNO, NO, NO_2^-, NO_3^-) and bio-relevant anions and cations (SO_4^{2-}, CH_3COO^-, Na^+, K^+, Mg^{2+}, Fe^{2+} and Cu^{2+}) (Figure 1B and D). No detectable emission increase was noted even when the probes were pre-incubated with a panel of 100 μM physiological analytes (1 mM for GSH). As a contrast, remarkable fluorescence enhancement was triggered by $ONOO^-$. A more intense study was carried out to examine the potential disturbance of hydrogen peroxide (H_2O_2), a known ROS reacting with α-keto compounds.[52,53] As shown in Figure S9, the fluorescence titration experiments show that both probes resist the interference of H_2O_2 with a broad concentration range from 0 to 1000 μM. The superior selectivity can be attributed to the much stronger nucleophilicity of $ONOO^-$ than H_2O_2, and thus the di-keto linker could resist H_2O_2. These results demonstrate that **Naph-ONOO$^-$** and **Rhod-ONOO$^-$** are feasible for $ONOO^-$ detection in

biological specimens.

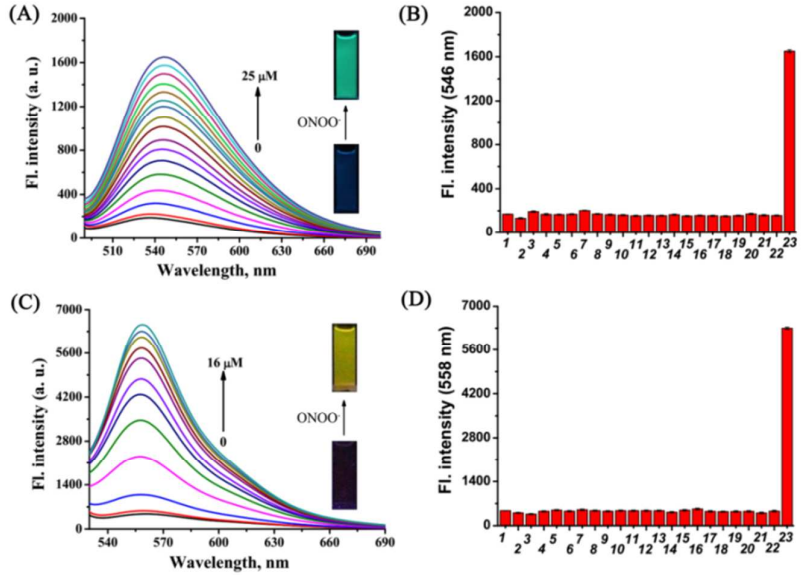

Figure 1. Fluorescence spectra of (A) **Naph-ONOO$^-$** and (C) **Rhod-ONOO$^-$** (5 μM) upon addition of $ONOO^-$ (0- 25 μM and 0-16 μM, respectively) in PBS buffer solution (25 mM, 1% DMF, pH 7.4); Fluorescence intensity of (B) **Naph-ONOO$^-$** and (D) **Rhod-ONOO$^-$** (5 μM) in PBS buffer solution (25 mM, 1% DMF, pH 7.4) toward various analytes: $ONOO^-$ (25 μM and 15 μM, respectively); other analytes (100 μM, 1 mM for GSH). 1, blank; 2, H_2O_2; 3, HOCl; 4, H_2S; 5, Cys; 6, GSH; 7, H_2S_2; 8, $O_2^{\bullet-}$; 9, HSO_3^-; 10, NO_2^-; 11, HNO; 12, NO; 13, NO_3^-; 14, CH_3COO^-; 15, BuOO•; 16, •OH; 17, Na^+; 18, K^+; 19, Mg^{2+}; 20, Fe^{2+}; 21, Cu^{2+}; 22, SO_4^{2-}; 23, $ONOO^-$. The mixture was kept for 40 min at room temperature before the fluorescence intensity of the probe solution was recorded. Excitation wavelength was 450 nm (A) and 500 nm (C), respectively.

Fluorescence imaging of exogenous/endogenous ONOO$^-$ generation in living cells. Encouraged by the above promising results *in vitro*, we further carried on with cellular bio-imaging of exogenous/endogenous $ONOO^-$ generation. Cytotoxicity measurements of both probes demonstrate that **Naph-ONOO$^-$** and **Rhod-ONOO$^-$** present minimal toxic effects on cell viability (Figure S10). To evaluate the efficacy of these probes on monitoring endogenously generated $ONOO^-$, we stimulated the cells with bacterial endotoxin lipopolysaccharide (LPS) and pro-inflammatory cytokine interferon-gamma (IFN-γ). These agents are known to trigger cellular apoptosis and release ROS/RNS, including $ONOO^-$.[54] To further validate the specificity of our probes, H_2O_2 and HOCl, both generated in large amount during apoptosis, were selected as the

representative interfering ROS in our studies. HepG2 cells were first stained with the fluorescent probes (**Naph-ONOO$^-$** and **Rhod-ONOO$^-$**), then treated with the stimulating reagents or control. As shown in Figure 2, when the cells were treated with control (PBS), they emitted negligible fluorescence signals. Similarly, H_2O_2 and HOCl-treated cells did not exhibit any marked fluorescence enhancement after incubation. Whereas as a sharp contrast, significant fluorescent increase was observed when cells were stimulated with LPS/IFN-γ, indicating that the increased signal was primarily due to the generated $ONOO^-$ during the stimulation. Furthermore, when the cells were pre-incubated with superoxide scavenger (2,2,6,6-tetramethylpiperidine-N-oxyl, TEMPO) or nitric oxide synthase inhibitor (aminoguanidine, AG), the generation of $ONOO^-$ was significantly reduced, as shown by the decreased fluorescence signals in HepG2 cells (Figure 2). These results evidence that our probes can specifically monitor low level of endogenously generated $ONOO^-$, without the interference from other ROS in living systems. Remarkably, because of the broad two-photon absorption action cross section exhibited by naphthalimide fluorophore (26 GM at 800 nm excitation) (Figure S11), fluorescent imaging for **Naph-ONOO$^-$** was also conducted under two-photon irradiation. **Naph-ONOO$^-$** thus can be applied for deep-tissue imaging of peroxynitrite.

Apart from the qualitative detection of $ONOO^-$, the quantitation or semi-quantitation is even more desired in screening assays. We next sought to semi-quantify the $ONOO^-$ generation using our probes. The HepG2 cells were incubated with both probes (5 μM) and the fluorescence intensities were recorded under either two-photon (TP) irradiation (800 nm, for **Naph-ONOO$^-$**) or one-photon (OP) irradiation (488 nm, for **Rhod-ONOO$^-$**) (Figure 3A and S12). Compared to the non-stimulated cells that exhibit very weak fluorescence, the pre-stimulated cells show a dose-dependent

fluorescence increase with different concentrations of LPS/IFN-γ (Figure 3A). Fluorescence intensity measurements indicate dynamic response range of the probes, as well as the potential to use fluorescence spectroscopy to conduct $ONOO^-$ quantitation. By recording the real-time peroxynitrite generation process in LPS-stimulated live cells, we confirmed that our probes can be used to monitor $ONOO^-$ for multiple purposes, including clinical research (Figure 3B and S13, S14). As a supporting test, we also demonstrated that these probes could be employed to image exogenous $ONOO^-$ by treating with 3-morpholinosydnonimine hydrochloride (SIN-1), an $ONOO^-$ generator (Figure S15 and S16). Importantly, **Naph-ONOO$^-$** and **Rhod-ONOO$^-$** can be applied to image $ONOO^-$ in other types of cell lines, such as HeLa cells and A549 cells (Figure S17 and S18). These features are very important to develop the fluorescent probes further into potent $ONOO^-$ assays and clinical trials.

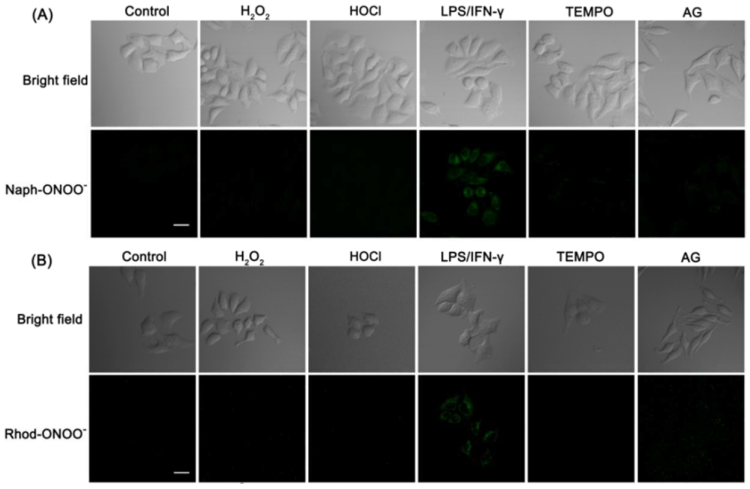

Figure 2. Pseudo-color fluorescence images of probes **Naph-ONOO$^-$** (A) and **Rhod-ONOO$^-$** (B) in HepG2 cells under different conditions by confocal fluorescence images. First column, cells were incubated with probe **Naph-ONOO$^-$** or **Rhod-ONOO$^-$** (5 μM, 40 min), respectively, then imaged; second-third column, cells were pretreated with probe **Naph-ONOO$^-$** or **Rhod-ONOO$^-$** (5 μM, 40 min), respectively, subsequently incubated with H_2O_2 (100 μM) (second column) or NaOCl (100 μM) (third column) for 30 min, then imaged; forth column, cells were pre-stimulated with LPS (1 μg/mL) and IFN-γ (50 ng/mL) for 12 hours, subsequently incubated with probe **Naph-ONOO$^-$** or **Rhod-ONOO$^-$** (5 μM, 40 min), respectively, then imaged; fifth-sixth column, cells pretreated

with $O_2^{\cdot-}$ scavenger TEMPO (300 μM) (fifth column) or NOS inhibitor AG (5 mM) (sixth column) during stimulation with LPS (1 μg/mL)/IFN-γ (50 ng/mL) for 12 hours, subsequently incubated with probe **Naph-ONOO⁻** or **Rhod-ONOO⁻** (5 μM, 40 min), respectively, then imaged. The fluorescence images were captured from the green channel of 500-570 nm with an excitation at 405 and 488 nm, respectively. First row: bright-field images. Second row: the fluorescence images of green channel collected at 500-570 nm. Scale bar: 20 μm.

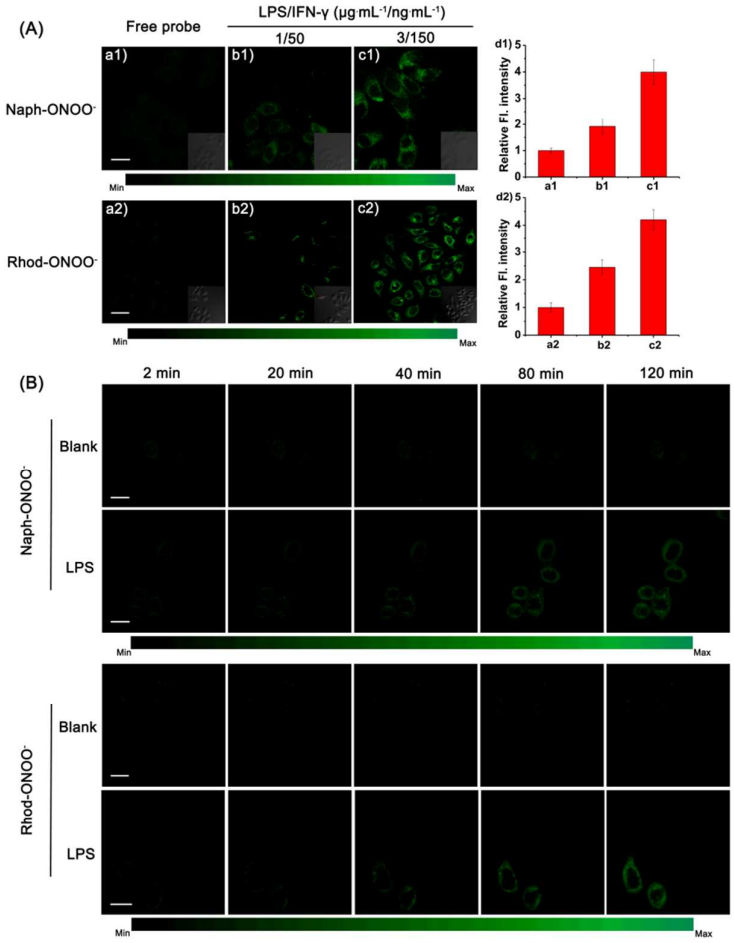

Figure 3. (A) Pseudo-color fluorescence images of $ONOO^-$ in HepG2 cells incubated with only **Naph-ONOO⁻** and **Rhod-ONOO⁻** (5.0 μM) (a) or co-incubated with different concentrations of LPS and IFN-γ (b-c). First column, cells were incubated with probe **Naph-ONOO⁻** or **Rhod-ONOO⁻** (5 μM, 40 min), then imaged; second and third column, cells were pre-stimulated with LPS/IFN-γ (1 $\mu g \cdot mL^{-1}$/50 $ng \cdot mL^{-1}$ or 3 $\mu g \cdot mL^{-1}$/150 $ng \cdot mL^{-1}$) for 12 hours, subsequently incubated with probe **Naph-ONOO⁻** or **Rhod-ONOO⁻** (5 μM, 40 min), then imaged. (d) Average intensity in a-c. Data are expressed as mean ± SD of three experiments. Excitation wavelength was 405 and 488 nm for the first and second row, respectively. The emission band was at 500-570 nm. Scale bar = 20 μm. (B) Real-time images of LPS-stimulated live cells. HepG2 cells were pretreated with **Naph-ONOO⁻** or **Rhod-ONOO⁻** (10 μM) for 20 min, and then with LPS (1 mg/mL, 50 μL). Excitation wavelength: 800 nm for **Naph-ONOO⁻** and 488 nm for **Rhod-ONOO⁻**. The emission band was at 500-560 nm for **Naph-ONOO⁻** and 500-570 nm for **Rhod-ONOO⁻**.

Scale bar = 20 μm.

Drug induced hepatotoxicity and remediation. To understand the cellular generation mechanism of peroxynitrite and to elaborate the drug-induced hepatotoxicity phenomenon, we proceeded to examine the $ONOO^-$ induced by commercially available drugs that are known to cause liver injury. It is reported that mitochondrial oxidative stress is a key source of ROS/RNS production.[51] Thus to examine the localization of our probes at subcellular levels, the cells were pre-treated with SIN-1, the $ONOO^-$ generator, then incubated with **Rhod-ONOO$^-$** and subsequently incubated with Mito-Tracker Red or Lyso-Tracker Red. As shown in Figure 4, the fluorescence of **Rhod-ONOO$^-$** accumulates within mitochondria and overlaps well with the signals of Mito-Tracker Red (overlap coefficient is 0.89) but not with Lyso-Tracker (Figure 4). The positively charged rhodamine fluorophore may be the main driving force of mitochondrial localization. On the other hand, **Naph-ONOO$^-$** is mainly dispersed within the cytoplasm. Hence it is not overlapping with either Mito-Tracker or Lyso-Tracker (Figure S19). We thus conclude that **Rhod-ONOO$^-$** should be more suitable for drug-induced hepatotoxicity measurements.

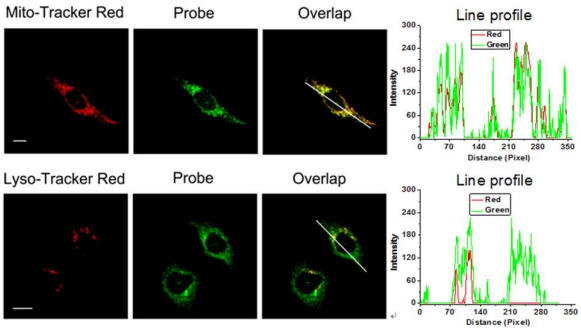

Figure 4. Intracellular localization of **Rhod-ONOO$^-$** in HepG2 cells. Images of HepG2 cells pre-treated with SIN-1 (100 μM, 2 hours), then incubated with 5 μM **Rhod-ONOO$^-$** for 40 min and subsequently 1 μM Mito-Tracker Red (or 1 μM Lyso-Tracker Red) for 10 min. Red channel: Mito-Tracker Red (λ_{ex}= 635 nm, λ_{em} = 600-675 nm) and Lyso-Tracker Red fluorescence (λ_{ex}= 559 nm, λ_{em} = 585-620 nm); green channel: probe fluorescence (λ_{ex} = 488 nm, λ_{em} = 500-570 nm); yellow: merged signal. Line profile: Intensity profile of the white line in image overlap. Scale bar: 10 μm.

Overdose of APAP is known to cause liver injury through enzymatic biotransformation that could result in the overproduction of $ONOO^-$.[12] Thus, efficient tracking of $ONOO^-$ during drug induced liver injury will benefit the deeper understanding of the hepatotoxicity mechanism. We first assessed the production of $ONOO^-$ with APAP. Cells were treated with APAP at a range of increasing concentrations (0-500 μM) for 12 hours, then incubated with **Rhod-ONOO$^-$** (5 μM) for 40 min. Apparently, the reaction based fluorescent probe is capable of trapping even trace amount of labile $ONOO^-$ generated through APAP-induced hepatotoxicity, as shown by the increased fluorescence signals (Figure 5A and B). The dose-dependent fluorescence intensities not only prove that $ONOO^-$ generation is correlated with APAP concentrations in cells, but also demonstrated the sensitivity of **Rhod-ONOO$^-$**. On the other hand, negligible fluorescence signals are observed with **Naph-ONOO$^-$** (Figure 5C and D). Because the colocalization experiments determine that **Naph-ONOO$^-$** accumulates mainly in cytoplasm (Figure S19),[55] these results suggest that $ONOO^-$ is mainly produced from mitochondrial oxidative stress during APAP drug stimulation. Furthermore, to test whether our probe can monitor $ONOO^-$ generation in real time, we recorded the fluorescence images at different time points. We first incubated the cells with **Rhod-ONOO$^-$**, then incubated with APAP, and imaged the cells at a set of times from 2 min to 120 min. As shown in Figure 5E and S20, fluorescence signals can already be seen from 80 min onwards, as compared to the negligible signals from cells without APAP stimulation (Figure S20). In addition, we also evaluated the level of $ONOO^-$ endogenously generated by other known DILI drugs (e.g. tetracycline and phenytoin). The results show that a significant reduced fluorescence intensity were observed comparing with APAP (Figure S21), demonstrating low level of $ONOO^-$ generation in the presence of tetracycline or phenytoin.

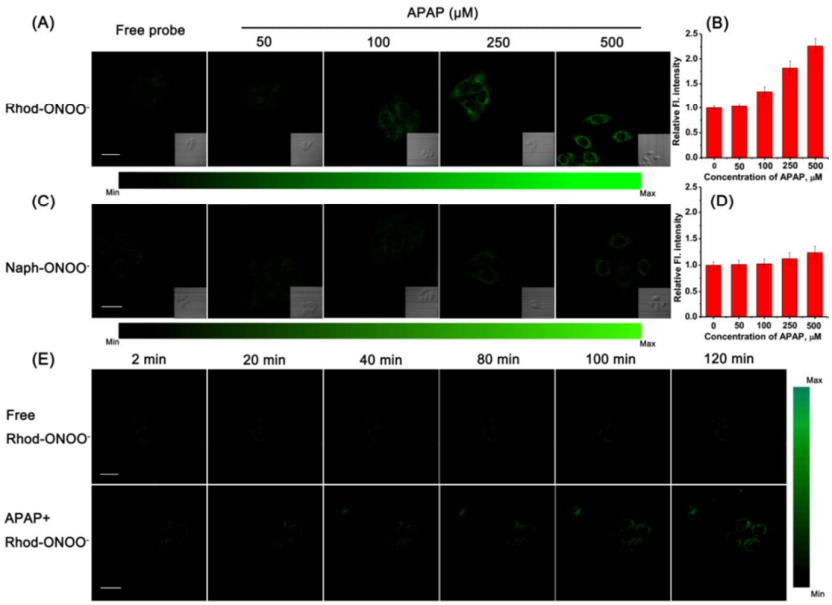

Figure 5. Pseudo-color fluorescence images of $ONOO^-$ in HepG2 cells incubated with only probes **Rhod-ONOO**$^-$ (A) and **Naph-ONOO**$^-$ (C) (5.0 μM) or co-incubated with different concentrations of APAP (0-500 μM) for 12 hours. First column, the HepG2 cells were treated with 5 μM **Rhod-ONOO**$^-$ or **Naph-ONOO**$^-$; second-fifth column, the HepG2 cells were pre-treated with different concentrations of APAP (50, 100, 250, 500 μM) for 12 hours, and then treated with 5 μM probe **Rhod-ONOO**$^-$ or **Naph-ONOO**$^-$ for 40 min. (B) and (D): Average intensity in Figure 5 (A) and (C), respectively. Data are expressed as mean ± SD of three experiments. Excitation wavelength was 488 nm (A) and 405 nm (C). The emission band was at 500-570 nm. Scale bar = 20 μm. (E) Real-time images of APAP-stimulated live cells. HepG2 cells were pretreated with **Rhod-ONOO**$^-$ (10 μM) for 20 min, and then with APAP (250 μM). Excitation wavelength was 488 nm. The emission band was at 500-570 nm. Scale bar = 20 μm.

Understanding the molecular pathway of drug induced hepatotoxicity can help researchers examine and ultimately avoid this phenomenon. Among the broad range of enzymes that could interact with drugs, cytochrome P450 families of oxidases are involved in xenobiotics metabolism in human bodies. The proposed mechanism for APAP induced hepatotoxicity involves CYP2E1-regulated oxidation of APAP to an iminoquinone, N-acetylparaquinonimine (NAPQI), which binds directly to proteins and causes the dysfunction of mitochondrial reactive species production[4] (Figure 6A). We hence predict that inhibiting either CYP2E1 enzyme or the whole CYP450 oxidase family should reduce $ONOO^-$ generation. Indeed, when the cells were

pre-incubated with trans-1,2-dichloroethylene (*t*-1,2-DCE; a specific inhibitor of CYP2E1[56]) during stimulation with APAP, downregulation of enzymatic activities significantly decreased the fluorescence intensities of **Rhod-ONOO$^-$**, as compared to the strong emission from control cells with only APAP stimulation. 1-Aminobenzotriazole (1-ABT; an inhibitor of CYP450 enzymes[56]), which can universally inhibit the CYP450 family oxidase, perform similarly to *t*-1,2-DCE by downregulating the enzyme activity (Figure 6B and C). These results corroborated the enzymatic pathways associated with APAP-induced hepatotoxicity for the first time with a small molecule fluorescent probe.

In addition, GSH is a potent antioxidant and nucleophilic scavenger of reactive metabolites (i.e., NAPQI and ROS-RNS[57]). We predict that adding GSH into the system should also quench the fluorescence of **Rhod-ONOO$^-$**. Indeed, observable fluorescence decrease was monitored with addition of GSH. However, the decrease was not as marked as the addition of enzyme inhibitors (Figure 6B and C). We proposed that it may due to the closer role of enzymatic pathways associated with APAP-induced hepatotoxicity than GSH. As a contrast, isoniazid (anti-tuberculosis agent, INH), another commercially available drug known to cause hepatotoxicity, was treated concomitantly to the cells with APAP. The fluorescence imaging exhibits that higher concentrations of INH indeed induce generation of more $ONOO^-$, as verified by our probe (Figure S22), and reveals the synergistic hepatotoxicity of combination therapy with APAP and INH. These results not only prove that our reaction based probe is very suitable for sensitive detection of $ONOO^-$ in situ, but also point out a potential pathway to elucidate the drug-induced hepatotoxicity process.

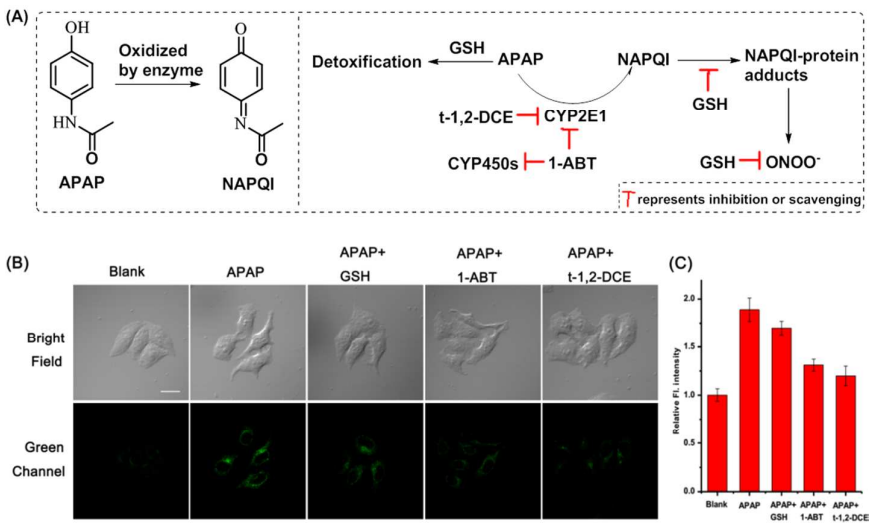

Figure 6. Fluorescent imaging remediation of APAP-induced hepatotoxicity with enzyme inhibitors and antioxidant scavengers in living HepG2 cells. (A) Mechanism of APAP-induced toxicity, with effects of inhibition by GSH, 1-ABT and *t*-1, 2-DCE. (B) Representative images of cells receiving from left to right: Blank, 250 μM APAP alone, and 250 μM APAP with GSH (200 μM), 1-ABT (160 μM), or *t*-1,2-DCE (20 μM), followed by **Rhod-ONOO**$^-$ (5 μM). (C) Average intensity in (B). Data are expressed as mean ± SD of three experiments. Excitation wavelength at 488 nm. The emission band at 500-570 nm. Scale bar = 20 μm.

Conclusion

Drug-induced hepatotoxicity has long affected public health, while its underlying molecular mechanism still remaining unsolved. With the newly designed, reaction based fluorescent probes, we have tried to investigate how ONOO$^-$ is generated and metabolized during the hepatotoxicity process. Based on the sensitive, biorthogonal deprotection of *a*-ketoamide, our probes enable the bioimaging and real-time monitoring of *in situ* generated peroxynitrite species. The selective ONOO$^-$ mediated nucleophilic reaction also ensures high specificity over other biological ROS and RNS. Remarkably, the reaction motif can be equipped with a range of fluorophores with diverse optical properties, as demonstrated by two-photon imaging of ONOO$^-$ with a naphthalimide probe **Naph-ONOO**$^-$.[58] The mitochondrial accumulation of another probe, **Rhod-ONOO**$^-$, reveals that peroxynitrite is mainly generated during drug induced oxidative stress within mitochondria. These

features allow us to investigate deeper into the molecular mechanism of drug-induced hepatoxicity. Through enzyme inhibitors and reactive metabolite scavengers, we for the first time imaged the $ONOO^-$ generation by CYP450 family oxidase-mediated xenobiotics metabolism. This study can be pushed further to pursue other enzymes or machinery associated with $ONOO^-$ generation. A potent fluorescence assay can also be formulated to monitor drug-induced hepatotoxicity in pre-clinical studies.

ACKNOWLEDGMENT

This work was financially supported by National Science Fund for Excellent Young Scholars (Grant 21622504), NSFC (Grant 21302050), the Foundation for Innovative Research Groups of NSFC (Grant 21521063), the Hunan University Fund for Multidisciplinary Developing (2015JCA04), and the Foundation of Hunan Educational Committee (Grant YB2016B037).

Supporting Information

Experimental details for chemical synthesis of all compounds, supplementary photophysical characterization of probes, and imaging methods and data. This material is available free of charge via the Internet at http://pubs.acs.org.

References

(1) Zimmerman, H. J., *Clin. Liver Dis.* **2000**, *4*, 73–96.

(2) Yuan, L.; Kaplowitz, N., *Clin. Liver Dis.* **2013**, *17*, 507–518.

(3) Chalasani, N.; Fontana, R. J.; Bonkovsky, H. L.; Watkins, P. B.; Davern, T.; Serrano, J.; Yang, H.; Rochon, J. *Gastroenterology*, **2008**, *135*, 1924–1934.

(4) Holt, M.; Ju, C. *Handb. Exp. Pharmacol.* **2010**, *196*, 3–27.

(5) Xu, J. J.; Diaz, D.; O'Brien, P. J. *Chem. Biol. Interact.* **2004**, *150*, 115–128.

(6) Dimasi, J. A. *Clin. Pharmacol. Ther.* **2001**, *69*, 297–307.

(7) Kola, I.; Landis, J. *Nat. Rev. Drug Discov.* **2004**, *3*, 711–715.

(8) Tengowski, M. W.; Kotyk, J. J. *Prog. Drug Res.* **2005**, *62*, 257–278.

(9) Hinson, J.; Roberts, D.; James, L., in *Adverse Drug Reactions*, Springer, Berlin, **2010**, *196*, 369–405.

(10) Bertolini, A.; Ferrari, A.; Ottani, A.; Guerzoni, S.; Tacchi, R.; Leone, S. *CNS Drug Rev.* **2006**, *12*, 250–275.

(11) Walsh, J. S.; Miwa, G. T. *Annu. Rev. Pharmacol. Toxicol.* **2011**, *51*, 145–167.

(12) Cover, C.; Mansouri, A.; Knight, T. R.; Bajt, M. L.; Lemasters, J. J.; Pessayre, D.; Jaeschke, H. *J. Pharmacol. Exp. Ther.* **2005**, *315*, 879–887.

(13) Radi, R. *J. Am.Chem. Soc.* **2013**, *288,* 26464–26472.

(14) Nagano, T. *J. Clin. Biochem. Nutr.* **2009**, *45*, 111–124.

(15) Mohar, I.; Stamper, B. D.; Rademacher, P. M.; White, C. C.; Nelson, S. D.; Kavanagh, T. J. *Redox Biology* **2014**, *2*, 377–387.

(16) Ducrocq, C.; Blanchard, B.; Pignatelli, B.; Ohshima, H. *Cell. Mol. Life Sci.* **1999**, *55,* 1068–1077.

(17) Masumoto, H.; Kissner, R.; Koppenol, W. H.; Sies, H. *FEBS Lett.* **1996**, *398,* 179–182.

(18) Zhang, H.; Liu, R.; Liu, J.; Li, L.; Wang, P.; Yao, S. Q.; Xu, Z.; Sun, H. *Chem. Sci.* **2016**, *7*, 256–260.

(19) Lee, M. H.; Kim, J. S.; Sessler, J. L. *Chem. Soc. Rev.* **2015**, *44*, 4185–4191.

(20) Ueno, T.; Nagano, T. *Nat. Methods.* **2011**, *8,* 642–645.

(21) Wan, Q. Q.; Chen, S. M.; Shi, W.; Li, L. H.; Ma, H. M. *Angew. Chem. Int. Ed.* **2014**, *53*, 10916–10920.

(22) Lin, V. S.; Chen, W.; Xian, M.; Chang, C. J. *Chem. Soc. Rev.* **2015**, *44*, 4596–4618.

(23) Yang, X.; Guo, Y.; Strongin, R. M. *Angew. Chem. Int. Ed.* **2011**, *50*, 10690–10693.

(24) Ferna ´ndez, A.; Vendrell, M. *Chem. Soc. Rev.* **2016**, *45*, 1182–1196.

(25) Yu, F.; Li, P.; Wang, B.; Han, K. *J. Am. Chem. Soc.* **2013**, *135*, 7674–7680.

(26) Li, J.; Yim, D.; Jang, W-D.; Yoon, J. *Chem. Soc. Rev.* **2017**, *46*, 2437–2458.

(27) Yang, D.; Tang, Y. C.; Chen, J.; Wang, X. C.; Bartberger, M. D.; Houk, K. N.; Olson, L. *J. Am. Chem. Soc.* **1999**, *121*, 11976–11983.

(28) Yang, D.; Wang, H. L.; Sun, Z. N.; Chung, N. W.; Shen, J. G. *J. Am. Chem. Soc.* **2006**, *128*, 6004–6005.

(29) Sun, Z. N.; Wang, H. L.; Liu, F. Q.; Chen, Y.; Tam, P. K. H.; Yang, D. *Org. Lett.* **2009**, *11*, 1887–1890.

(30) Peng, T.; Yang, D. *Org. Lett.* **2010**, *12*, 4932–4935.

(31) Chang, M. C. Y.; Pralle, A.; Isacoff, E. Y.; Chang, C. J. *J. Am. Chem. Soc.* **2004**, *126*, 15392–15393.

(32) Oushiki, D.; Kojima, H.; Terai, T.; Arita, M.; Hanaoka, K.; Urano, Y.; Nagano, T. *J. Am. Chem. Soc.* **2010**, *132*, 2795–2801.

(33) Zhou, M.; Diwu, Z.; Panchuk-Voloshina, N.; Haugland, R. P. *Anal. Biochem.* **1997**, *253*, 162–168.

(34) Setsukinai, K. I.; Urano, Y.; Kikuchi, K.; Higuchi, T.; Nagano, T. *J. Chem. Soc., Perkin Trans.* **2000**, *2*, 2453–2457.

(35) Wardman, P. *Free Radical Biol. Med.* **2007**, *43*, 995–1022.

(36) Shepherd, J.; Hilderbrand, S. A.; Waterman, P.; Heinecke, J. W.; Weissleder, R.; Libby, P. *Chem. Biol.* **2007**, *14*, 1221–1231.

(37) Panizzi, P.; Nahrendorf, M.; Wildgruber, M.; Waterman, P.; Figueiredo, J. L.; Aikawa, E.; McCarthy, J.; Weissleder, R.; Hilderbrand, S. A. *J. Am. Chem. Soc.* **2009**, *131*, 15739–15744.

(38) Zhang, Q.; Zhu, Z.; Zheng, Y.; Cheng, J.; Zhang, N.; Long, Y-T.; Zheng, J.; Qian, X.; Yang, Y. *J. Am. Chem. Soc.* **2012**, *134*, 18479–18482.

(39) Peng, T.; Wong, N. K.; Chen, X.; Chan, Y. K.; Ho, D. H.; Sun, Z.; Hu, J. J.; Shen, J.; El-Nezami, H.; Yang, D. *J. Am. Chem. Soc.* **2014**, *136*, 11728–11734.

(40) Cheng, D.; Pan, Y.; Wang, L.; Zeng, Z. B.; Yuan, L.; Zhang, X. B.; Chang, Y. T. *J. Am. Chem. Soc.* **2017**, *139*, 285–292.

(41) Peng, T.; Chen, X.; Gao, L.; Zhang, T.; Wang, W.; Shen, J.; Yang, D. *Chem. Sci.* **2016**, *7*, 5407–5413.

(42) He, X.; Li, L.; Fang, Y.; Shi, W.; Lia, X.; Ma, H. *Chem. Sci.* **2017**, *8*, 3479–3483 .

(43) Peng, J.; Samanta, A.; Zeng, X.; Han, S.; Wang, L.; Su, D.; Loong, D. T. B.; Kang, N-Y.; Park, S-J.; Homayoun All, A.; Jiang, W.; Yuan, L.; Liu, X.; Chang, Y-T. *Angew. Chem. Int. Ed.* **2017**, *56*, 4165−4169.

(44) Montoya, L. A.; Pluth, M. D. *Chem. Commun.* **2012**, *48*, 4767–4769.

(45) Sakabe, M.; Asanuma, D.; Kamiya, M.; Iwatate, R. J.; Hanaoka, K.; Terai, T.; Nagano, T.; Urano, Y. *J. Am. Chem. Soc.* **2013**, *135*, 409−414.

(46) Sun, Q.; Yang, S-H.; Wu, L.; Dong, Q-J.; Yang, W-C.; Yang, G-F. *Anal. Chem.* **2016**, *88*, 6084−6091.

(47) Areti, S.; Verma, S. K.; Bellare, J.; Rao, C. P. *Anal. Chem.* **2016**, *88*, 7259−7267.

(48) Feng, S.; Liu, D.; Feng, W.; Feng, G. *Anal. Chem.* **2017**, *89*, 3754–3760.

(49) Li, M.; Feng, W.; Zhai, Q.; Feng, G. *Biosens. Bioelectron.* **2017**, *87*, 894–900.

(50) Zhang, L.; Zhu, H.; Zhao, C-C.; Gu, X-F. *Chin. Chem. Lett.* **2017,** *28*, 218–221.

(51) Xu, W.; Zeng, Z. B.; Jiang, J-H.; Chang, Y-T.; Yuan, L. *Angew. Chem. Int. Ed.* **2016**, *55*, 13658–13699.

(52) Xie, X.; Yang, X.; Wu, T.; Li, Y.; Li, M.; Tan, Q.; Wang, X.; Tang, B. *Anal. Chem.* **2016**, *88*, 8019–8025.

(53) Abo, M.; Urano, Y.; Hanaoka, K.; Terai, T.; Komatsu, T.; Nagano, T. *J. Am. Chem. Soc.* **2011**, *133*, 10629–10637.

(54) Knight, T. R.; Kurtz, A.; Bajt, M. L.; Hinson, J. A.; Jaeschke, H. *Toxicol. Sci.* **2001**, *62*, 212–220.

(55) Srikun, D.; Miller, E. W.; Domaille, D. W.; Chang, C. J. *J. Am. Chem. Soc.* **2008**, *130*, 4596–4597.

(56) Jackson, T. E.; Lilly, P. D.; Recio, L.; Schlosser, P. M; Medinsky, M. A. *Toxicol. Sci.* **2000**, *55*, 266–273.

(57) James, L. P.; McCullough, S. S.; Lamps, L.W.; Hinson, J. A. *Toxicol. Sci.* **2003**, *75*, 458–467.

(58) Similar result was reported during the preparation of this manuscript: Li, Y.; Xie, X.; Yang, X.; Li, M.; Jiao, X.; Sun, Y.; Wang, X.; Tang, B. *Chem. Sci.* **2017**, *8*, 4006–4011.

TOC:

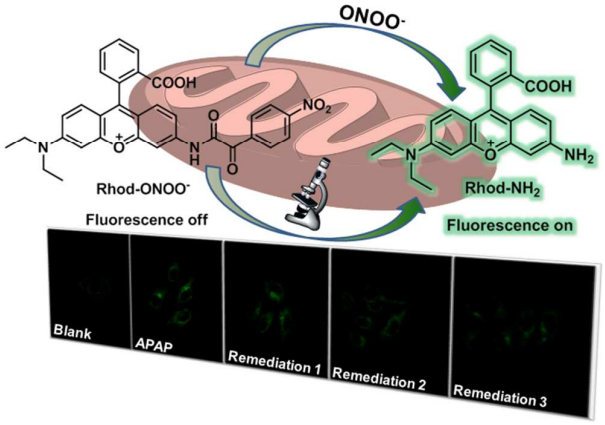
ONOO-
COOH
NO2
O
N
H
O
N
O+
Rhod-ONOO-
Fluorescence off
COOH
NH2
N
O+
Rhod-NH2
Fluorescence on
Blank
APAP
Remediation 1
Remediation 2
Remediation 3